Unsupervised Domain Adaptation via Spatial Pattern Alignment for VEP-based Identity Recognition

Hongze Zhao[1], Yijun Wang[1], and Xiaorong Gao[1]

[1]Affiliation not available

April 08, 2024

Unsupervised Domain Adaptation via Spatial Pattern Alignment for VEP-based Identity Recognition

Hongze Zhao, Yijun Wang*, *Member, IEEE*, Xiaorong Gao*, *Member, IEEE*

***Abstract*—Electroencephalography (EEG) biometrics has garnered significant attention in recent years owing to its non-intrusive nature, real-time detection capabilities, concealment, and high complexity. Despite these promising attributes, the practical deployment of EEG-based identity recognition systems remains hindered by limited cross-day recognition performance. While some studies have reported cross-day recognition, they often suffer from slow recognition speeds, failing to meet the basic requirements for practical applications. To address this issue, we propose an unsupervised domain adaptation algorithm based on spatial pattern alignment for visual-evoked potential (VEP)-based identity recognition. This method employs rotational alignment of spatial patterns to correct cross-day spatial filters and utilizes forward selection to identify optimal sub-bands. By utilizing this approach, significant improvements of speed and accuracy in cross-day recognition can be achieved. We validate the proposed algorithm on three existing VEP datasets: Dataset I (25 subjects across 30 days), Dataset II (21 subjects across 5 days), and Dataset III (15 subjects across 200 days). The results demonstrate a significant superiority over the compared algorithms. Furthermore, we conduct online experiments with 15 individuals across over 1000 days, and the outcomes remain consistent. Analyzing the dataset over nearly three years in terms of temporal dimension, we observe evident template aging effect: 30 days > 200 days > 1000 days. However, the proposed method effectively mitigates template aging, resulting in minimal performance differences among the various datasets. The introduced algorithm substantially enhances speed and accuracy in cross-day recognition, paving the way for the long-term stability and practicality of online brainwave recognition systems.**

***Index Terms*—Electroencephalography, Biometrics, Transfer Learning, Domain Adaptation, Aging Effect.**

This work was supported by the National Key R&D Program of China under grant 2022YFF1202303 and the National Natural Science Foundation of China under grant 62071447, U2241208 and Key R&D Program of Ningxia Hui Autonomous Region under grant 2023BEG02063.

H. Zhao and X. Gao are with Department of Biomedical Engineering, School of Medicine, Tsinghua University, Beijing, 100084, China (email: zhaohz23@mails.tsinghua.edu.cn, gxr-dea@mail.tsinghua.edu.cn).

Y. Wang is with the State Key Laboratory on Integrated Optoelectronics, Institute of Semiconductors, Chinese Academy of Sciences, Beijing, 100083, China (email: wangyj@semi.ac.cn).

Correspondence authors (asterisks): Yijun Wang and Xiaorong Gao.

I. INTRODUCTION

IN today's highly digitized and interconnected society, the security of identity information is of paramount importance for both individuals and society. Biometric methods such as fingerprint identification, facial authentication, and iris detection have become commonplace of security authentication in daily life. However, these methods still exhibit certain security vulnerabilities [1]. For instance, due to the natural secretion of oils by the human body, fingerprints are prone to being left behind and could potentially be acquired by malicious individuals for illicit purposes, such as gummy fingers, thus compromising security protocols [2]. Similarly, facial authentication is not foolproof in ensuring liveness detection, as it can be deceived by methods like using masks [3]. Additionally, iris detection could be deceived by contact lenses engraved with iris patterns [4]. In contrast, electroencephalography (EEG)-based recognition, with its characteristics of excellent concealment, high complexity, and live detection, is considered to overcome the aforementioned drawbacks and is widely regarded as a more secure biometric method [5-7]. Furthermore, its portability, non-invasiveness, and cost-effectiveness in data collection [8] have contributed to its increasing popularity. However, existing research has yet to fully meet the requirements for practical real-world applications, as it often suffers from slow recognition speed and template aging effects, with very few deployments of online systems [8].

Most of the earlier studies in EEG biometrics [9-13] have primarily reported excellent speed and accuracy of within-day recognition; however, it remains unknown whether the cross-day recognition performance aligns with the requirements of practical scenarios. Subsequent studies reported satisfactory cross-day recognition accuracy [8], [14-18], yet the persistent challenge of slow recognition speed has hindered practical implementation [19], [20]. The primary cause of poor cross-day recognition lies in the non-stationarity of EEG signals, where data collected at different times exhibit variations due to factors like lighting conditions, electrode placement, and impedance [17]. This is a common challenge in long-term brain-computer interface (BCI) research [21], often referred as transductive transfer learning, where the source domain has labeled data, but the target domain's labels are unknown, yet tasks are the same across domains [22].

On one hand, in research of steady-state visual evoked potentials (SSVEP), several studies have explored novel methodologies in transfer learning. For instance, Yuan et al

utilized transfer template-based canonical correlation analysis (ttCCA) to transfer templates from other subjects, significantly enhancing SSVEP detection accuracy [23]. They also developed an online algorithm, online transfer template-based CCA (ott-CCA), which adaptively updates the EEG templates. Nakanishi et al employed a least-squares template reconciliation (LST)-based TRCA method to effectively improve cross-device SSVEP detection accuracy [24]. In [25], [26], the Align and Pool for EEG Headset Domain Adaptation (ALPHA) method was employed, resulting in enhanced SSVEP detection accuracy across electrodes and days.

On the other hand, in the realm of emotion recognition, numerous cross-day investigations have been conducted. For example, in [27], Chai et al employed subspace alignment (SA) on six publicly available datasets to detect three types of emotion, achieving impressive outcomes. Additionally, cross-day research plays a pivotal role in motor imagery studies. In [28], He and Wu employed Euclidean-space alignment (EA) for motor imagery classification, surpassing Riemannian space-based methods and attaining commendable results. However, to the best of our knowledge, such research is rare in the context of EEG-based identity recognition [29], [30].

To bridge this gap and achieve domain adaptation for enhancing cross-day performance, we propose a domain adaptation algorithm based on spatial pattern alignment for visual-evoked potential (VEP)-based identity recognition. In particular, we adjust spatial filters that have been initially trained on the source domain by leveraging unlabeled data from the target domain. This process aims to enhance their alignment with the target domain, consequently leading to an enhancement in classification accuracy. Additionally, we optimize the selection of sub-bands using a forward selection approach, which enhancing cross-day performance on existing data. Finally, we validate the effectiveness of the algorithm through online experiments, demonstrating consistency with established dataset performance levels.

The innovations and contributions of this paper include: (1) introducing a novel unsupervised domain adaptation algorithm based on spatial pattern alignment, which reduces differences between data distributions of different sessions; (2) proposing a forward selection-based parameter optimization method that improves cross-day performance; (3) achieving excellent performance on three cross-day datasets; (4) establishing an online experimental system that validates the algorithm's online performance; (5) showcasing the algorithm's significant impact in mitigating the template aging issue.

The subsequent sections of the paper are structured as follows. The Methodology section details the mathematical expression of the proposed algorithm, parameter optimization methods, and performance evaluation strategies. The Results section presents comprehensive cross-day results, feature analysis, and parameter analysis across various datasets. The Discussion section outlines the limitations of this work and suggests future research directions. The Conclusion section summarizes the main achievements of the paper.

II. METHODS

A. Template-matching Framework

In our previous studies on VEP-based person identification [8, 31], we employed a template-matching classification method based on spatial filtering algorithms. Here, we provide a brief overview. We begin by preprocessing the raw EEG data in several steps:

1. Extracting data epochs from the raw EEG data based on event triggers.
2. Establishing a consistent starting point for stimuli by considering a 0.14s delay in the visual pathway [32].
3. Downsampling the data from 1000Hz to 250Hz.
4. Correcting baseline by subtracting the data's mean value.
5. Applying a filter bank method [33] using Chebyshev Type I filters to divide the data into multiple sub-bands.

Subsequently, we proceed with the training phase (enrollment step). After subjecting all first-day data (labeled as X_s) to the aforementioned preprocessing steps, we utilize the algorithm framework depicted in Figure 1. For each sub-band, canonical correlation analysis (CCA) algorithm is independently applied to compute spatial filters, resulting in the creation of signal templates (average waveforms). This process forms the EEG template library, with each subject possessing their corresponding spatial filters and EEG templates. Finally, the testing phase (identification step) involves processing unknown identity data (labeled as X_t in Figure 1). We multiply the spatial filters of all subjects and apply the proposed Align Spatial Pattern (ASP) algorithm with the unknown data. Then we compute the correlation coefficient r between them and the spatially filtered EEG templates. This yields a set of features representing the correlation between the unknown data and templates of each subject. The subject with the highest feature value is determined as the identity of the unknown data. Notably, for cases involving multiple trials (N), our approach computes an independent feature value r for each trial (i) and then aggregates them to represent the features of the entire signal segment $R = \sum_{i=1}^{N} r_i$.

B. Task-Related Component Analysis (TRCA)

TRCA (Task-Related Component Analysis) is a spatial filtering method used to effectively extract task-related components by maximizing signal reproducibility during the task period [34]. TRCA is frequently employed in classification of SSVEP signals [35]. The basic assumption is that the signals can be divided into two source spaces: (1) task-related signals $s(t) \in \mathbb{R}$ and (2) task-unrelated signals $n(t) \in \mathbb{R}$. The linear observation model for multi-channel EEG signals $\boldsymbol{x}(t) \in \mathbb{R}^{N_c}$ is represented as:

$$x_j(t) = a_{1,j}s(t) + a_{2,j}n(t), j = 1,2, \dots, N_c \quad (1)$$

Here, j represents the channel index, and $a_{1,j}$ and $a_{2,j}$ are coefficients that project the source signals onto the EEG signals. For solving the task-related component $s(t)$ from the linear observation signal $\boldsymbol{x}(t)$, the equation is expressed as:

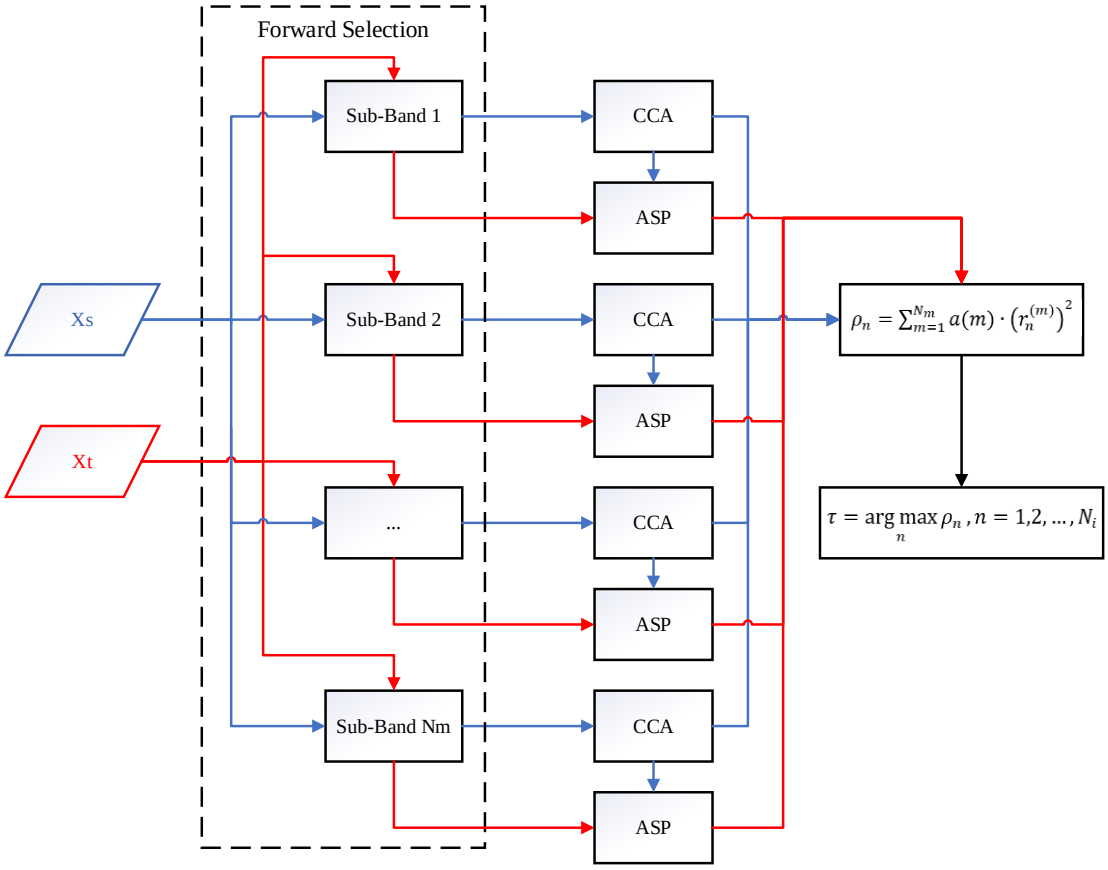

Figure 1. Flow chart of the identification algorithm: the algorithm integrates filter bank analysis with spatial filter algorithm based on a template-matching approach, where CCA stands for Canonical Correlation Analysis and ASP stands for Spatial Pattern Alignment. This amalgamation aims to identify the subject by detecting code-modulated VEP.

$$\begin{aligned} y(t) &= \sum_{j=1}^{N_c} w_j x_j(t) \\ &= \sum_{j=1}^{N_c} \left(w_j a_{1,j} s(t) + w_j a_{2,j} n(t) \right) \end{aligned} \tag{2}$$

Ideally, the solution to the equation should satisfy $\sum_{j=1}^{N_c} w_j a_{1,j} = 1$ and $\sum_{j=1}^{N_c} w_j a_{2,j} = 0$, resulting in $y(t) = s(t)$. In practice, this equation could be solved by maximizing the inter-trial covariance. For the EEG signals of the h-th trial and the estimated task-related component, denoted as $\boldsymbol{x}^{(h)}(t)$ and $y^{(h)}(t), h = 1,2,\ldots,N_t$, the duration of $y^{(h)}(t)$ is fixed within $t \in [t_h, t_h + T]$, where T is the duration of each trial. The correlation coefficient between $h1$ and $h2$ of $y(t)$ is expressed as:

$$\begin{aligned} C_{h_1 h_2} &= \mathrm{Cov}\left(y^{(h_1)}(t), y^{(h_2)}(t) \right) \\ &= \sum_{j_1, j_2 = 1}^{N_c} w_{j_1} w_{j_2} \mathrm{Cov}\left(x_{j_1}^{(h_1)}(t), x_{j_2}^{(h_2)}(t) \right). \end{aligned} \tag{3}$$

The sum over all possible combinations of trials is given by:

$$\begin{aligned} \sum_{\substack{h_1, h_2 = 1 \\ h_1 \neq h_2}}^{N_t} C_{h_1 h_2} &= \sum_{\substack{h_1, h_2 = 1 \\ h_1 \neq h_2}}^{N_t} \sum_{j_1, j_2 = 1}^{N_c} w_{j_1} w_{j_2} \mathrm{Cov}\left(x_{j_1}^{(h_1)}(t), x_{j_2}^{(h_2)}(t) \right) \\ &= \boldsymbol{w}^T \boldsymbol{S} \boldsymbol{w}. \end{aligned} \tag{4}$$

The matrix $\boldsymbol{S} = \left(S_{j_1 j_2} \right)_{1 \le j_1, j_2 \le N_c}$ is defined as:

$$S_{j_1 j_2} = \sum_{\substack{h_1, h_2 = 1 \\ h_1 \neq h_2}}^{N_t} \mathrm{Cov}\left(x_{j_1}^{(h_1)}(t), x_{j_2}^{(h_2)}(t) \right). \tag{5}$$

To obtain a feasible solution, we constrained the variance of $y(t)$:

$$\begin{aligned} \mathrm{Var}\left(y(t) \right) &= \sum_{j_1, j_2 = 1}^{N_c} w_{j_1} w_{j_2} \mathrm{Cov}\left(x_{j_1}(t), x_{j_2}(t) \right) \\ &= \boldsymbol{w}^T \boldsymbol{Q} \boldsymbol{w} \\ &= 1 \end{aligned} \tag{6}$$

The solution to this constrained optimization problem is:

$$\widehat{\boldsymbol{w}} = \arg\max_{\boldsymbol{w}} \frac{\boldsymbol{w}^T \boldsymbol{S} \boldsymbol{w}}{\boldsymbol{w}^T \boldsymbol{Q} \boldsymbol{w}}. \tag{7}$$

The largest eigenvector of the matrix $\boldsymbol{Q}^{-1}\boldsymbol{S}$ is the optimal spatial filter, and the correlation coefficient is calculated between the EEG template and the projected test data as shown in Equation (8):

$$r_n^{(m)} = \rho\left(\overline{\boldsymbol{X}}^{(m)^T} \boldsymbol{w}_n^{(m)}, \overline{\boldsymbol{X}}_n^{(m)^T} \boldsymbol{w}_n^{(m)} \right) \tag{8}$$

C. Align Spatial Pattern Algorithm (ASP)

Inspired by [25], we apply the ASP algorithm to brainwave recognition. Specifically, we first use template-based CCA to obtain spatial filters SF_s and SF_t. Corresponding spatial patterns could then be obtained using Equation (9):

$$\begin{aligned} SP_s &= SF_s^{-T} \\ SP_t &= SF_t^{-T} \end{aligned} \tag{9}$$

We believe that the changes in spatial patterns caused by the non-stationarity of brainwave signals can be corrected through rotational symmetry. Therefore, we need to use the estimated spatial pattern SP_t to find an orthogonal transformation matrix Q that aligns SP_s, as defined in the optimization problem of Equation (10):

$$\begin{aligned} &\underset{Q}{minimize} \quad ||SP_s - SP_t Q^T||_F^2 \\ &s.t. \quad QQ^T = I \end{aligned} \tag{10}$$

The equation belongs to the typical Orthogonal Procrustes Problem [37]. The solution is given by multiplying the left (L) and right (R) singular vectors of $SP_s{}^T SP_t$, resulting in:

$$Q = LR^T \tag{11}$$

Then, we can obtain the transformed spatial filter:

$$SF^{ASP} = SF_t Q^T \tag{12}$$

In practical usage, we modify the method of obtaining spatial filters $SF_{X_s\bar{X}}$ for training data to be $CCA(X_s, \overline{X_s})$, and the method of obtaining spatial filters $SF_{X_t\bar{X}}$ for test data to be $CCA(X_t, \overline{X_s})$. The alignment process is similar to the above procedure, and the method of obtaining correlation coefficients is defined by Equation (13):

$$R = corr(SF_{X_s\bar{X}}\bar{X}_s, SF_{X_t\bar{X}}^{ASP^T} X_t) \tag{13}$$

D. Parameter Optimization

As mentioned earlier, we commonly use a filter bank approach [33] in the template-matching framework with a structure shown in Figure 2. The weights are typically determined using the empirical formula from [33]: $a(m) = m^{-1.25}+0.25$. However, this formula may not be universally suitable, prompting some studies to perform search and optimization [38]. In this paper, we initially adopt the grid search method from [31] to optimize parameters of the filters, which starts by searching for the lower and upper limits of the basic band, and then a grid search is performed to determine the number of filters and their frequency intervals.

Furthermore, we introduce a novel frequency band selection algorithm based on Forward Selection [39]. The approach involves individually classifying the features of each sub-band to obtain accuracy results: $ACCsb_1$, $ACCsb_2$, ..., $ACCsb_n$. For each sub-band, a curve is plotted using the data length (number of trials) as the x-axis and accuracy as the y-axis. The area under the curve (AUC) is used as the evaluation metric, denoted as Score. The algorithm begins by selecting the sub-band with the highest Score as the first frequency band. Subsequently, the combination of two sub-bands, which contains each band merged with the first frequency band, with the highest Scores is selected, and this process continues iteratively. The algorithm stops when the Score no longer increases or increases by less than 0.0001. Once the frequency bands are selected through forward selection, the weights of all selected frequency bands are set to 1, resulting in the final set of parameters.

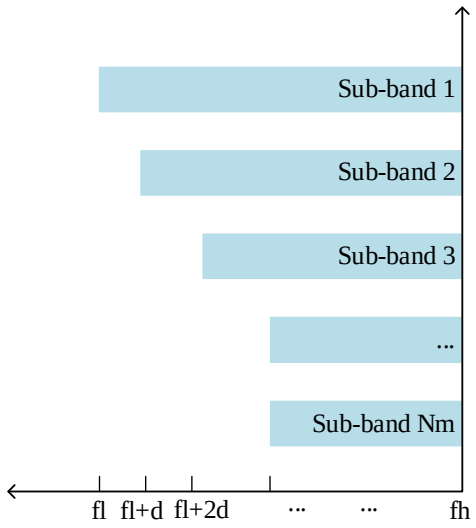

Figure 2. Representative frequency structure for all sub-bands in filter bank design. Here, 'fl' and 'fh' denote the lower and upper bounds of frequencies, respectively, with 'd' representing the frequency interval between two adjacent sub-bands.

Algorithm 1. Forward Sub-band Selection

Input: Sub-band 1, sub-band 2, …, sub-band N_m

Process:

I. Calculate the score for each individual sub-band.

II. Sort the scores in descending order and select the highest one (S1).

III. Calculate the score for each pair combination with S1.

IV. Sort the scores of the combinations in descending order and select the highest one (S1-S2).

...

V. Repeat the process until the score either stabilizes or increases by less than 0.0001.

Output: Selected combination of sub-bands [a, b, c, ...]

E. Performance Evaluation

(1) Existing Datasets: We have accumulated a significant amount of data in our previous studies. In [31], we collected cross-day data from 25 individuals. The recording channels included 9 electrodes in the occipital region (Pz, PO3/4, PO5/6, POz, Oz, and O1/2), with an average interval of 30 days between sessions. The stimulation consisted of 63-bit M-sequences, and each trial lasted 1.05 seconds. There were 8 different stimulation modes (M1-M6, Mx4, Mx6). This dataset is referred to as 'Dataset I'. In another study [8], we collected cross-day data from 21 individuals and compared the effectiveness of three types of Visual Evoked Potentials

(VEP): Flash VEP (FVEP), Steady-State VEP (SSVEP), and Code-modulated VEP (CVEP) for identity recognition. Each trial lasted 1.05 seconds, and the average time interval between sessions was 5 days. This dataset is referred to as 'Dataset II'. We also conducted online experiments on 15 participants from the [31] study, using a stimulus sequence of M5 and an average time span of 200 days. The templates for this experiment were taken from the first day (D1) of Dataset I. This dataset is labeled as 'Dataset III'. These studies achieved promising results, and for more details, please refer to the original papers [8], [31]. We will now use these datasets to evaluate the performance of the proposed algorithm. The characteristics of these datasets are summarized in Table 1.

Table 1. Details of three existing cross-day CVEP datasets

Dataset	Number of subjects	Time span (average)	References
Dataset I	25	30 days	[31]
Dataset II	21	5 days	[8]
Dataset III	15	200 days	[8]

(2) Online Experiment: In addition to the existing datasets mentioned above, we conducted new online experiments with recruited participants. We invited 15 participants from Dataset II to participate in online experiments. This group consisted of 4 males and 11 females, with an average age of 28.3 (ranging from 26 to 31). The average time interval between their initial participation and the online experiment was 1009 days (ranging from 1001 to 1017 days). All participants had normal or corrected-to-normal vision. Each participant read and signed an informed consent form approved by the Institution Review Board of Tsinghua University (NO. 20230058) before the experiment. For the online experiment, we used the stimulus pattern described in [8], specifically the CVEP-M5 sequence, and the experimental setup is depicted in Figure 3. The online recognition process involved real-time feedback based on the algorithm's output, which presented the participant's identity. Each participant underwent an offline experiment consisting of 100 trials for in-day evaluation before proceeding to an online experiment involving 50 runs (with a total of 500 trials). A run comprised 10 trials, and after each run, the system provided feedback on the recognition result. The inter-trial rest time was 0.7 seconds, and there was a pause between two consecutive runs. Participants could resume the experiment by pressing the space bar when they were ready. The electrode positions for data collection were the classic occipital region with 9 channels, as described above. We refer to this dataset as '3Y'.

(3) Performance Assessment: For parameter optimization, we employed a classical wrapper method [40], which means all our optimizations were based on the cross-day recognition results of the 25 individuals' data from [31], specifically using the M5 stimulation mode. The obtained algorithm parameters were then applied to other datasets. Performance evaluation primarily focused on comparing cross-day accuracy under equivalent data lengths. We used five domain adaptation

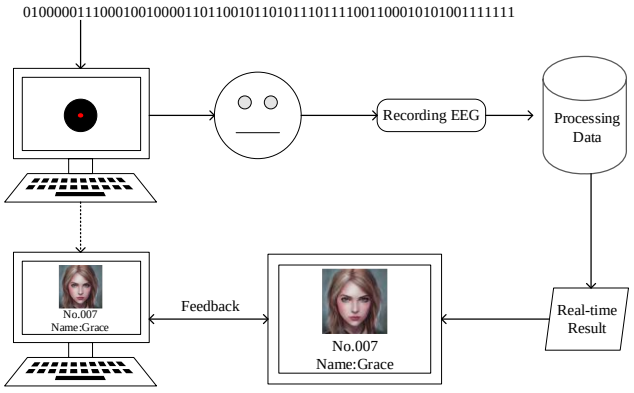

Figure 3. Diagram of the online VEP-based brainwave recognition system.

algorithms suitable for this paradigm as benchmarks. Individual Template Canonical Correlation Analysis (itCCA) is a widely-used classification algorithm in BCI applications. Based on CCA, it seeks linear combinations of brain signals that maximize correlation with corresponding intentions or actions, facilitating classification and decoding of brain signals [36]. Least Squares Template (LST) reconciliation is another commonly used technique that aims at estimating and correcting differences by fitting a linear model. It has been employed to enhance the classification performance of SSVEP in cross-device scenarios [24]. Euclidean Alignment (EA) is a popular data alignment method used to align data from different sources or devices into a common reference framework. It operates by mapping data onto a common Euclidean space, enabling alignment of data collected from diverse sources or devices to similar positions within this space [28]. Kernel Principal Component Analysis (KPCA) is a nonlinear extension of traditional PCA, widely applied for dimensionality reduction and feature extraction across various domains, including pattern recognition, image processing, and machine learning. This algorithm is commonly employed as a transfer learning method. TRCA is the method we used for individual identification in our previous research [8], [31]. All cross-day performance evaluations were conducted using the first day's data for training and the second day's data for testing, with no overlaps by any algorithm. Additionally, we utilized in-day performance as reference in some cases. For in-day classification accuracy, we employed the TRCA algorithm (as in-day results rapidly saturate, with minimal differences among algorithms) using leave-one-out cross-validation, i.e., using a sliding window to pick n trials for testing and using the remaining (100-n) trials for training.

(4) Feature Evaluation: We performed an analysis of the effectiveness of the ASP algorithm features. First, we analyzed the R^2 feature values [35] , [41]. We compared two scenarios: using ASP-based alignment with feature value $R1 = \mathrm{corr}(SF_{X_s\bar{X}}\bar{\mathrm{X}}_s, \mathrm{SF}_{X_t\bar{X}}^{ASP^T}\mathrm{X}_t)$ and using CCA without ASP, resulting in feature value $R2 = \mathrm{corr}(SF_{X_s\bar{X}}\bar{\mathrm{X}}_s, SF_{X_s\bar{X}}\mathrm{X}_t)$. For visualization purposes, we applied t-distributed stochastic neighbor embedding (t-SNE) [42] to project the feature distributions of several typical participants into a lower-dimensional space.

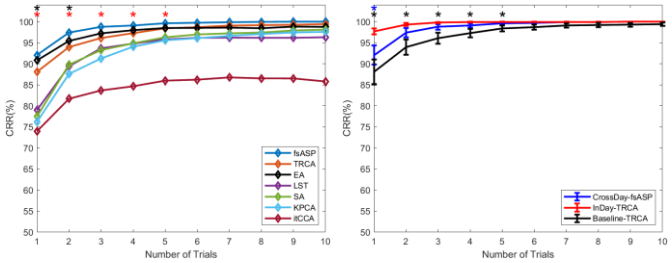

(a) (b)

Figure 4. Dataset I's performance comparison of (a) fsASP and other comparative methods in cross-day identification, where black stars indicate the significance of fsASP compared to EA (black), while red stars indicate the significance of fsASP compared to TRCA (red), (b) fsASP in cross-day identification, TRCA in cross-day and within-day identification, where blue stars indicate the significance of InDay-TRCA compared to CrossDay-fsASP (blue), while black stars indicate the significance of InDay-TRCA compared to Baseline-TRCA(black).

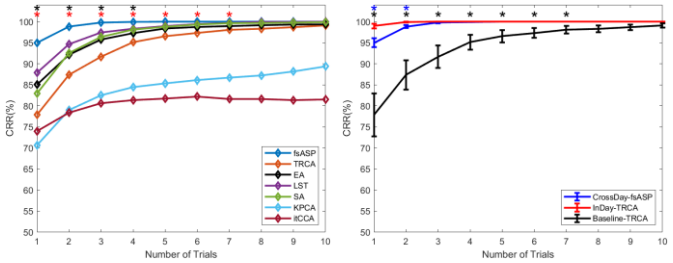

(a) (b)

Figure 5. Dataset II's performance comparison of (a) fsASP and other comparative methods in cross-day identification, where black stars indicate the significance of fsASP compared to EA (black), while red stars indicate the significance of fsASP compared to TRCA (red), (b) fsASP in cross-day identification, TRCA in cross-day and within-day identification, where blue stars indicate the significance of InDay-TRCA compared to CrossDay-fsASP (blue), while black stars indicate the significance of InDay-TRCA compared to Baseline-TRCA(black).

(5) Filter Bank: As previously mentioned, using a filter bank is a common approach in BCIs to enhance performance, and weighting coefficients are determined empirically [33]. Here, we applied the proposed method to reselect and optimize filter bank parameters. Then, we compared the performance of the classical setup against that of the forward selection.

III. Results

1. Performance Evaluation

Dataset I (with 25 Participants across 30 Days): As shown in figure 4(a), we compared the cross-day recognition accuracy of various algorithms for the M5 stimulus. It's evident that the accuracy obtained using fsASP (Forward Selection combing Align Spatial Pattern) is superior to other benchmark algorithms. Paired t-test demonstrated significant superiority of fsASP over TRCA for 1 to 5 trials (p-values: 0.0322, 0.0129, 0.0312, 0.0253, 0.0349). For 1 to 2 trials, fsASP outperformed EA significantly (p-values: 0.0036, 0.0321), while no significant difference was observed between EA and TRCA. fsASP achieved a cross-day accuracy of 92.08% with 1 trial, 99.63% with 5 trials, and 100% with 10 trials, signifying a remarkable improvement in cross-day recognition. All fsASP results were achieved using the optimal parameters specific to each scenario, which will be elaborated on in subsequent sections. Here, we first present the parameters used: all fsASP subspace numbers (N_k) are set to 4, sub-band weighting coefficients are all set to 1, the number of sub-bands [8] for M5 is 3, which decided by forward selection, and filter group parameters chosen are [4, 93], [20, 93], [24, 93]. These parameters are also used for subsequent results. LST, SA, and KPCA exhibited similar performance results, with no significant differences among them 1-10 trials: $p > 0.05$), and paired t-tests indicated that all three were significantly lower than TRCA, LST vs TRCA: $p < 0.0001$ (1-trial), $p < 0.01$ (2-trials); SA vs TRCA: $p < 10^{-5}$ (1-trial), $p < 0.01$ (2-trials), $p < 0.05$ (3-trials); KPCA vs TRCA: $p < 10^{-5}$ (1-trial), $p < 0.001$ (2-trials), $p < 0.01$ (3-trials), $p < 0.05$ (4-trials). However, itCCA demonstrated the poorest performance, significantly worse than all other methods. In figure 4(b), a comparison between fsASP results, TRCA results as the baseline, and in-day recognition using the TRCA algorithm is presented. The results show that fsASP outperformed the baseline, with a significantly reduced gap between cross-day and in-day recognition accuracy, and no significant difference was observed between 2 and 10 trials.

Dataset II (with 21 Participants across 5 Days): In figure 5(a), we conducted a similar analysis on Dataset II using the CVEP (M5) stimulus. The results demonstrate significant improvement in cross-day recognition achieved by the proposed algorithm. Specifically, the proposed fsASP algorithm significantly outperformed the TRCA algorithm in cross-day recognition accuracy for 1 to 7 trials (1-trial: $p < 0.001$, 2 and 3 trials: $p < 0.01$, 4 to 7 trials: $p < 0.05$), which achieved a cross-day accuracy of 94.98% with 1 trial, and 100% accuracy with 5 and 10 trials. Paired t-tests results indicated no significant difference between LST, EA, and SA (1-10 trials: $p > 0.05$), while paired t-tests showed that their performance was significantly lower than fsASP: fsASP vs LST: $p < 0.01$ (1 and 3 trials), $p < 0.05$ (2, 4, 5 trials); fsASP vs SA: $p < 0.001$ (1 trial), $p < 0.01$ (2 to 4 trials), $p < 0.05$ (5 trials); fsASP vs EA: $p < 0.01$ (1 to 3 trials), $p < 0.05$ (4 trials). However, itCCA and KPCA exhibited relatively poorer performance. Figure 5(b) presents a comparison between fsASP results, TRCA results as the baseline, and in-day recognition using the TRCA algorithm on Dataset II. It's clear that the proposed algorithm significantly improved cross-day recognition accuracy compared to the baseline. Additionally, fsASP achieved results close to in-day recognition, with only minor differences observed. Significant differences were observed only in 1-2 trials, and the accuracy differences were less than 5%.

Dataset III (with 15 Participants across 200 Days): Figure 6(a) depicts the results obtained from the online experiment with 15 participants across 200 days in Dataset III. Training was conducted using Dataset I data, while the online experiment data were utilized for testing purposes. The results show a significant enhancement in cross-day recognition accuracy achieved by the proposed fsASP algorithm. Specifically, the fsASP algorithm outperformed TRCA significantly in 1 to 2 trials (p-values: 0.0017 and 0.031). While fsASP showed no significant difference compared to EA, it demonstrated slightly higher accuracy than EA for 3 to 10 trials. The fsASP algorithm achieved a cross-day

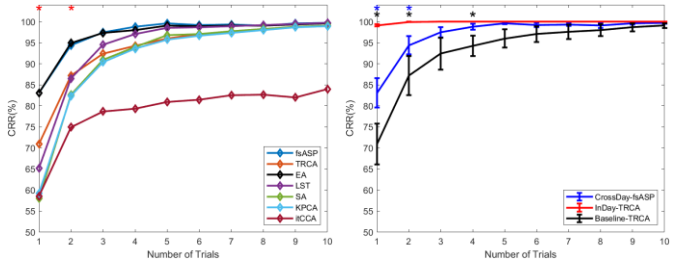

(a) (b)

Figure 6. Dataset III's performance comparison of (a) fsASP and other comparative methods in cross-day identification, where black stars indicate the significance of fsASP compared to EA (black), while red stars indicate the significance of fsASP compared to TRCA (red), (b) fsASP in cross-day identification, TRCA in cross-day and within-day identification, where blue stars indicate the significance of InDay-TRCA compared to CrossDay-fsASP (blue), while black stars indicate the significance of InDay-TRCA compared to Baseline-TRCA(black).

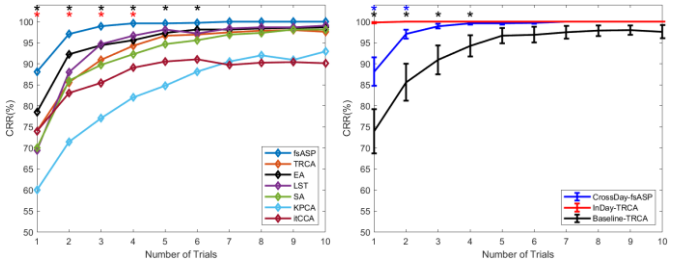

(a) (b)

Figure 7. 3Y dataset's performance comparison of (a) fsASP and other comparative methods in cross-day identification, where black stars indicate the significance of fsASP compared to EA (black), while red stars indicate the significance of fsASP compared to TRCA (red), (b) fsASP in cross-day identification, TRCA in cross-day and within-day identification, where blue stars indicate the significance of InDay-TRCA compared to CrossDay-fsASP (blue), while black stars indicate the significance of InDay-TRCA compared to Baseline-TRCA(black).

recognition accuracy of 83.07% with 1 trial, 99.60% with 5 trials, and 99.73% with 10 trials. P indicated no significant difference between LST, TRCA, SA, and KPCA (1-10 trials: $p > 0.05$), while itCCA continued to exhibit significantly lower performance compared to all other methods. As shown in figure 6(b), we compared the in-day and cross-day recognition accuracy. Using TRCA results as the baseline, the results demonstrate a significant improvement brought by the proposed algorithm compared to the baseline. Furthermore, the gap between cross-day and in-day performance is substantially reduced by fsASP, with no significant difference between cross-day and in-day performance for trials 3 to 10.

3Y (with 15 Participants across 1000 Days): The performance evaluation was conducted on the newly collected online experiment data referred to as the 3Y dataset. Training was carried out using the CVEP-M5 from Dataset II to create templates. The average cross-day recognition accuracies for the 15 participants are depicted in figure 7(a). The results indicate that the proposed algorithm significantly outperforms other methods. Paired t-tests revealed that, for 1 to 4 trials, fsASP is significantly better than TRCA ($p < 0.01$ for 1-trial, $p < 0.05$ for 2-4 trials), and for 1 to 6 trials, it is significantly better than EA ($p < 0.01$ for 1-trial, $p < 0.05$ for 2-6 trials). fsASP achieved a cross-day recognition accuracy of 88.13% with 1 trial, 99.60% with 5 trials, and 100% with 10 trials. EA, LST, TRCA, and SA exhibited no significant differences in their results, whereas itCCA still performed poorly and KPCA had lower performance levels in the first 6 trials. Comparative results between in-day and cross-day recognition are shown in figure 7(b), with TRCA serving as the baseline. The results indicate a significant enhancement in cross-day performance by fsASP compared to the baseline, and a substantial reduction in the gap between cross-day and in-day performance. For trials 3 to 10, the cross-day performance of fsASP is comparable to in-day performance.

Initially, parameter optimization was performed using the Dataset I featuring M5 stimuli. Subsequently, the optimized parameters were applied to the Dataset II, Dataset III, and 3Y datasets. The performance evaluation across all four datasets consistently demonstrated the superior performance of the fsASP algorithm in cross-day recognition compared to the contrastive algorithms. Noticeably, the fsASP algorithm not only significantly improved cross-day recognition accuracy but also effectively narrowed the performance gap between cross-day and in-day recognition, particularly when compared against TRCA as the baseline. Notably, when the number of trials exceeded three, the cross-day performance of the fsASP algorithm exhibited no significant difference from the in-day performance. However, it is noteworthy that while EA and LST algorithms exhibited relatively enhanced performance compared to the TRCA algorithm, their improvement effects were not consistently stable, implying that their performance improvements are limited under specific circumstances, potentially leading to performance degradation. In contrast, the effectiveness of SA and KPCA algorithms in enhancing performance is not universally observed, possibly due to their shared utilization of the PCA subspace decomposition method, which may exhibit suboptimal performance in certain contexts. Conversely, the itCCA algorithm consistently demonstrated inferior performance to the TRCA algorithm across all scenarios, suggesting its subpar classification proficiency.

2. Feature Evaluation

(1) R^2 Evaluation: On the 3Y dataset, we compared the distribution of R^2 values before and after employing the ASP algorithm. As depicted in figure 8(a), there is a substantial enhancement in the self-correlation values across the 15 participants. Simultaneously, as shown in figure 8(b), there is a slight improvement in the average correlation values between individuals (others). Further analysis of the enhancement magnitudes for these two types of correlations, presented in figure 8(c), reveals a significant difference in favor of self-correlation enhancement ($p < 0.001$). This observation underscores that the utilization of the ASP algorithm leads to a notable increase in feature value disparities, consequently contributing to the enhancement of classification performance.

(2) t-SNE Evaluation: We conducted t-SNE analysis on a subset of individuals from the 3Y dataset who exhibited substantial enhancement. In figure 9, the red points represent the centers of training data, the green points depict the feature distribution prior

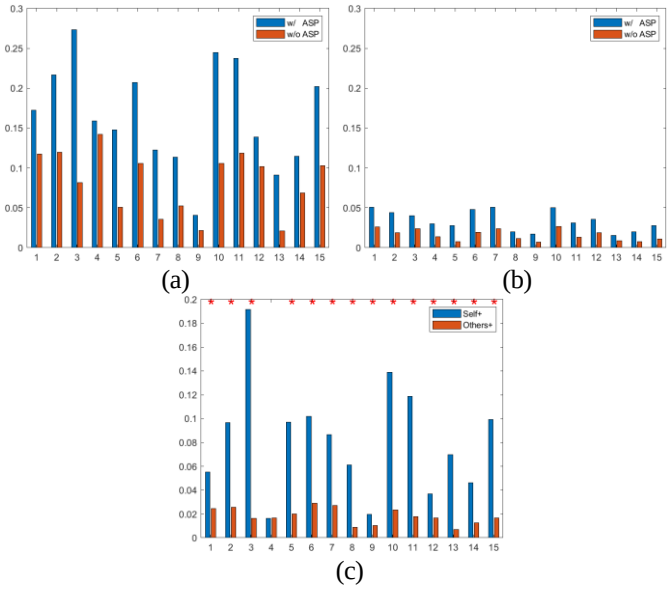

Figure 8. The R-squared statistics for correlation coefficients of (a) Target self-correlation with or without ASP, (b) Non-target average correlation with or without ASP, and (c) improvement of self-correlation applying ASP.

to applying the ASP algorithm, and the blue points illustrate the feature distribution post-ASP algorithm application. Clearly visible is the phenomenon where the feature distribution before applying the proposed ASP algorithm is more dispersed. However, with the use of the ASP algorithm, the feature distribution becomes more concentrated around the central region, simplifying the classification task and thereby contributing to the improvement of cross-day recognition performance.

3. Filter Bank

Employing the classical feature selection technique of forward selection, we further optimized the grid-params (fliter bank parameters decided by grid search method from [31]). The

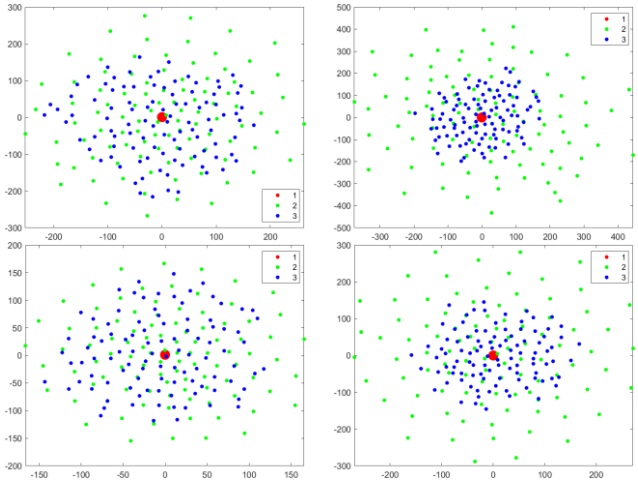

Figure 9. The low dimensional feature space projected by t-SNE of four typical subjects. The embeddings of training data are represented by red dots, and the feature distribution before/after applying the ASP algorithm are represented by green/blue dots. The test embeddings are moved toward the template embeddings with the help of ASP algorithm.

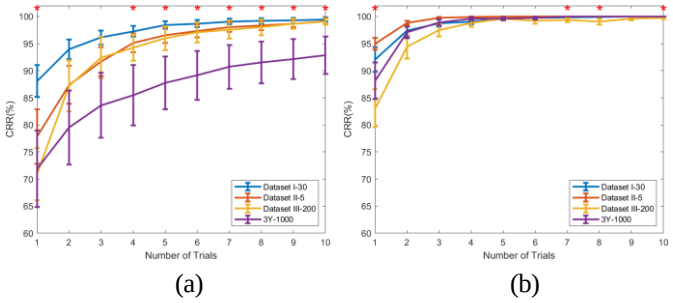

Figure 10. All datasets' performance comparison of using (a) TRCA algorithm, and (b) fsASP algorithm in cross-day identification.

outcome of this optimization yielded a set of parameters, denoted as 'fs-params', consisting of 3 filter sub-bands with parameters [4, 93], [20, 93], [24, 93], all weighted equally at 1. A comparison of results is presented in Table 2, indicating a noticeable improvement in performance across all datasets when using fs-params as compared to grid-params. Notably, the largest enhancement was observed in the 3Y dataset, with an average increase of approximately 0.3% (average of gap) in cross-day recognition accuracy.

4. Template Aging Analysis

We conducted a template aging analysis using the four datasets. Dataset II and 3Y share the same training template, originating from the first day's (D1) data of the same group of subjects. However, they differ in the interval between data collection. Dataset II has an average interval of 5 days (D1-D2: 5 days), whereas 3Y exhibits an average interval of more than 1000 days (D1-D3: 1009 days). Applying the existing algorithm framework, we observed pronounced template aging effects, with a significant overall decline in performance for the 3Y dataset compared to Dataset II, particularly evident in the 5-10 trial range. Furthermore, as depicted in figure 10(a), there exists a strong consistency between the order of cross-day recognition accuracy and the length of time intervals. Specifically, the order of performance is Dataset I-30 >Dataset III-200 > 3Y-1000, with statistical significance observed across 1, 3-10 trials. But when considering Dataset II, the regularity and statistical significance slightly diminishes, although its intervals are only 5 days, which are not on the same order of magnitude as the intervals of the other datasets. On the other hand, the results achieved using the proposed fsASP algorithm demonstrate similar performance levels across all datasets as shown in figure 10(b). ANOVA analysis indicates no significant differences in the 2-6, and 9 trial range, suggesting that the fsASP algorithm partially mitigates the effects of template aging. Further paired t-test suggests that Dataset II-5 significantly outperformed 3Y-1000 in 1 trial situation ($p < 0.05$) and Dataset III-200 in 1-3, 5, 7 trials situation ($p < 0.05$), Dataset I-30 significantly outperformed Dataset III-200 in 1 and 8 trials situation ($p < 0.05$), and 3Y-1000 significantly outperformed Dataset III-200 in 1 trial situation ($p < 0.05$).

Table 2. Four dataset's performance comparison in cross-day identification with grid search parameters or forward selection parameters.

Acc (%)	**Dataset I**			**Dataset II**			**Dataset III**			**3Y**		
Trial	grid-params	fs-params	gap	grid-params	fs-params	gap	grid-params	fs-params	gap	grid-params	fs-params	gap
1	92.6000	92.0800	-0.5200	95.6567	94.9765	-0.6803	82.5333	83.0667	**0.5333**	88.4000	88.1333	-0.2667
2	96.8485	97.4141	**0.5657**	99.1104	98.8488	-0.2616	95.0667	94.4000	-0.6667	96.2667	97.0667	**0.8000**
3	98.4898	98.7755	**0.2857**	99.6860	99.7907	**0.1047**	97.0667	97.4667	**0.4000**	98.4000	98.9333	**0.5333**
4	99.0103	99.0928	**0.0825**	99.8953	99.9477	**0.0523**	98.2667	98.8000	**0.5333**	98.9333	99.6000	**0.6667**
5	99.3333	99.6250	**0.2917**	99.9477	100.0000	**0.0523**	99.0667	99.6000	**0.5333**	99.0667	99.6000	**0.5333**
6	99.4526	99.7474	**0.2947**	99.9477	100.0000	**0.0523**	99.6000	99.2000	-0.4000	99.6000	99.7333	**0.1333**
7	99.4894	99.8723	**0.3830**	100.0000	100.0000	0.0000	99.7333	99.3333	-0.4000	99.6000	100.0000	**0.4000**
8	99.6559	99.9570	**0.3011**	100.0000	100.0000	0.0000	99.7333	99.0667	-0.6667	99.8667	100.0000	**0.1333**
9	99.5652	100.0000	**0.4348**	100.0000	100.0000	0.0000	99.8667	99.6000	-0.2667	99.8667	100.0000	**0.1333**
10	99.6923	100.0000	**0.3077**	100.0000	100.0000	0.0000	99.7333	99.7333	0.0000	100.0000	100.0000	0.0000

IV. Discussion

We introduced an EEG biometric recognition algorithm based on ASP, which demonstrated significant improvements across all four datasets. Concerning the filter bank, we introduced a novel parameter optimization method that led to performance improvements. Originally, the filter bank structure was inspired by SSVEP-based spelling classification [33], [35], [43], [44]. SSVEP stimuli are characterized by frequency-phase locking, where both the fundamental and harmonic frequencies are predictable. For instance, in a 10Hz SSVEP stimulus, responses can be predicted for the fundamental frequency at 10Hz and harmonic frequencies at 20Hz, 30Hz, 40Hz, and so on. Therefore, the structure illustrated in Figure 2 is logical and effective, with filter parameters like [8, 92], [18, 92], [28, 92], etc. However, we utilized a CVEP stimulation mode depicted in Figure 11, in which case, responses exhibit an approximately broadband signal profile, and there is no decay in harmonic frequencies. Consequently, the optimized filter parameters we obtained actually represent more concentrated frequency ranges of the stimulus. Additionally, the intensity differences between adjacent frequency bands are not substantial. To reflect this, we adopted equal weighting. Interestingly, as shown in Table 2, in a few cases, the results using fs-params showed slight decreases: Dataset I: 1-trial, Dataset II: 1st and 2nd trials, Dataset III: 2nd, 6th, 7th, 8th, and 9th trials, 3Y: 1-trial. This can be explained by the fact that a weighting factor of 1 is not necessarily optimal, and there remains marginal room for fine-tuning. However, our rationale behind this approach lies in significantly reducing computational complexity. While grid-params required 7 sub-bands, fs-params only needed 3 sub-bands, resulting in a reduction of computational load to less than half. This reduction is of paramount importance for real-time communication, system implementation, and enabling online deployment of EEG biometric recognition systems in practical scenarios.

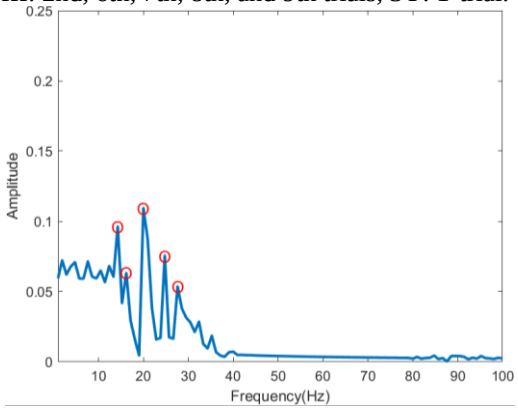

Figure 11. Amplitude responses for a typical c-VEPs.

Our proposed algorithm significantly enhances cross-day recognition performance in EEG biometric identification while narrowing the performance gap between in-day and cross-day scenarios. Furthermore, it effectively alleviates the template aging phenomenon. Particularly, under single-trial conditions, which last approximately 1 second, our existing system achieved a cross-day recognition accuracy of nearly 90%. In terms of performance, to the best of our knowledge, this stands as the current best online performance level, and the potential implications of achieving 90% accuracy in just 1 second are considerable. This allows for the possibility of integrating our system into BCIs, where communication and authentication occur concurrently, ensuring personal information security and user privacy in BCI systems. Moreover, the integration of BCI systems and brain biometric recognition doesn't burden the users any further, as the stimulation tasks can be carried out simultaneously. This combination has the potential to achieve encrypted communication through brainwave signals, thereby enhancing information confidentiality and resistance to attacks, which, in turn, bolsters the security of BCI systems.

Our ASP-based algorithm operates under the assumption that spatial patterns can be aligned through rotation. This assumption is both a mathematical premise and a deduction from practical experimental operations. During EEG data collection, efforts are made to maintain the relative stability of EEG cap positions (e.g., measuring distances front-to-back, checking left-right symmetry, ensuring minimal deviation in electrode coverage, etc.). However, slight differences are inevitable due to variations in the penetration and diffusion of conductive gel (as we employ wet electrodes), slight disparities in EEG cap shapes, and varying levels of electrode contact quality and participants' hair thickness. The

algorithm's corrective measures hold practical significance. The spatial pattern variations are an aspect deserving further research attention. Future studies could include higher electrode densities to cover larger brain areas [45], potentially leading to more comprehensive mathematical models with enhanced interpretability and precision. Furthermore, other algorithms under certain conditions also have the potential to yield improvements, such as EA, LST, etc. In the future, we intend to develop integrated algorithms to further enhance performance, provided the complexity remains acceptable.

We conducted an analysis of template aging effects using data spanning intervals of over 1000 days. Our proposed algorithm effectively mitigated this phenomenon. However, our research has been limited to several types of VEP signals, including classic SSVEP and various CVEP modes. The universality of the proposed algorithm requires further exploration and extension. For instance, applying it to resting-state signals like RO or RC, or ERP signals elicited by RSVP stimuli, and the promising AEP signals, which have shown promising performance of identity recognition in recent years. Our study was based on datasets involving 15-25 participants, with the longest time span being 1000 days, and the stimulation modes being somewhat limited. There are existing studies with larger participant numbers and longer spans, e.g., with over 100 participants' data in [11], spanning three years with multiple stages in [17], encompassing cross-day data for 12 different stimuli in [46]. Therefore, we aim to collect larger datasets, delve into longer-term template aging effects, and explore their implications.

V. Conclusion

We have introduced an ASP-based domain adaptation algorithm employing spatial pattern alignment and forward selection. This approach substantially enhances cross-day recognition accuracy and speed in VEP-based person identification. We validated our method on three existing datasets (Dataset I: 25 participants across 30 days, Dataset II: 21 participants across 5 days, Dataset III: 15 participants across 200 days) as well as a newly acquired online experiment dataset (3Y: 15 participants across 1000 days). The results of the proposed algorithm consistently outperform the existing TRCA algorithm and other comparative methods. Template aging effects were evident in the original framework: 30 days > 200 days > 1000 days. However, the proposed method effectively mitigates this template aging effect, resulting in near-equal performance across all datasets. The algorithm's substantial enhancement of cross-day recognition accuracy offers the potential for the deployment of online EEG biometric recognition systems towards long-term use.

Acknowledgment

The authors would like to express special gratitude to B. Liu for his invaluable advice on algorithmic aspects.

References

[1] K.P. Thomas and A.P. Vinod, *Toward EEG-Based Biometric Systems: The Great Potential of Brain-Wave-Based Biometrics.* IEEE Syst. Man Cybern. Mag., 2017. **3**(4): p. 6-15.

[2] H.M. Tsutomu Matsumoto, Koji Yamada, Satoshi Hoshino, *Impact of artificial "gummy" fingers on fingerprint systems*, in *Optical Security and Counterfeit Deterrence Techniques IV*. 2002. p. 275-289.

[3] J. Galbally and R. Satta, *Three-dimensional and two-and-a-half-dimensional face recognition spoofing using three-dimensional printed models.* IET Biom., 2016. **5**(2): p. 83-91.

[4] G. Kaur, G. Singh, and V. Kumar, *A review on biometric recognition.* International Journal of Bio-Science and Bio-Technology, 2014. **6**(4): p. 69-76.

[5] R. Palaniappan and D.P. Mandic, *Biometrics from Brain Electrical Activity: A Machine Learning Approach.* IEEE Trans. Pattern Anal. Mach. Intell., 2007. **29**(4): p. 738-742.

[6] D.S. Bassett and M.S. Gazzaniga, *Understanding complexity in the human brain.* Trends Cognit. Sci., 2011. **15**(5): p. 200-209.

[7] P. Campisi and D. La Rocca, *Brain waves for automatic biometric-based user recognition.* IEEE Trans. Inf. Forensics Secur., 2014. **9**(5): p. 782-800.

[8] H. Zhao, Y. Chen, W. Pei, et al., *Towards online applications of EEG biometrics using visual evoked potentials.* Expert Syst. Appl., 2021. **177**.

[9] R. Palaniappan, *Method of identifying individuals using VEP signals and neural network.* IEE Proceedings - Science, Measurement and Technology, 2004. **151**(1): p. 16-20.

[10] K. Das, S. Zhang, B. Giesbrecht, et al., *Using Rapid Visually Evoked EEG Activity for Person Identification.* 2009 Annual International Conference of the Ieee Engineering in Medicine and Biology Society, Vols 1-20, 2009: p. 2490-2493.

[11] D.L. Rocca, P. Campisi, B. Vegso, et al., *Human Brain Distinctiveness Based on EEG Spectral Coherence Connectivity.* IEEE Trans. Biomed. Eng., 2014. **61**(9): p. 2406-2412.

[12] M.V. Ruiz-Blondet, Z. Jin, and S. Laszlo, *CEREBRE: A Novel Method for Very High Accuracy Event-Related Potential Biometric Identification.* IEEE Trans. Inf. Forensics Secur., 2016. **11**(7): p. 1618-1629.

[13] B.-K. Min, H.-I. Suk, M.-H. Ahn, et al., *Individual Identification Using Cognitive Electroencephalographic Neurodynamics.* IEEE Trans. Inf. Forensics Secur., 2017. **12**(9): p. 2159-2167.

[14] M. Kostilek and J. Stastny, *EEG biometric identification: repeatability and influence of movement-related EEG.* 2012 International Conference on Applied Electronics, 2012: p. 147-150.

[15] B.C. Armstrong, M.V. Ruiz-Blondet, N. Khalifian, et al., *Brainprint: Assessing the uniqueness, collectability, and permanence of a novel method for ERP biometrics.* Neurocomputing, 2015. **166**: p. 59-67.

[16] R. Das, E. Maiorana, and P. Campisi, *EEG Biometrics Using Visual Stimuli: A Longitudinal Study*. IEEE Signal Process Lett., 2016. **23**(3): p. 341-345.

[17] E. Maiorana and P. Campisi, *Longitudinal Evaluation of EEG-Based Biometric Recognition.* IEEE Trans. Inf. Forensics Secur., 2018. **13**(5): p. 1123-1138.

[18] D.H. Sherif Nagib Abbas Seha, *Longitudinal Assessment of EEG Biometrics under Auditory Stimulation A_Deep Learning Approach*, in *EUSIPCO*. 2021.

[19] R. Saia, S. Carta, G. Fenu, et al., *Influencing brain waves by evoked potentials as biometric approach: taking stock of the last six years of research.* Neural Computing and Applications, 2023. **35**(16): p. 11625-11651.

[20] R.S. Harshit, Kavitha P Thomas, Smitha K. G. and A. P. Vinod, *Online Electroencephalogram (EEG) based biometric authentication using visual and audio stimuli*, in *2016 IEEE EMBS Conference on Biomedical Engineering and Sciences*. 2016.

[21] K.-J. Chiang, C.-S. Wei, M. Nakanishi, et al., *Boosting template-based SSVEP decoding by cross-domain transfer learning.* J. Neural Eng., 2021. **18**(1).

[22] Z. Wan, R. Yang, M. Huang, et al., *A review on transfer learning in EEG signal analysis.* Neurocomputing, 2021. **421**: p. 1-14.

[23] P. Yuan, X. Chen, Y. Wang, et al., *Enhancing performances of SSVEP-based brain–computer interfaces via exploiting inter-subject information.* J. Neural Eng., 2015. **12**(4).

[24] M. Nakanishi, Y.-T. Wang, C.-S. Wei, et al., *Facilitating Calibration in High-Speed BCI Spellers via Leveraging Cross-Device Shared Latent Responses.* IEEE Trans. Biomed. Eng., 2020. **67**(4): p. 1105-1113.

[25] B. Liu, X. Chen, X. Li, et al., *Align and Pool for EEG Headset Domain Adaptation (ALPHA) to Facilitate Dry Electrode Based SSVEP-BCI.* IEEE Trans. Biomed. Eng., 2022. **69**(2): p. 795-806.

[26] X. Liu, B. Liu, G. Dong, et al., *Facilitating Applications of SSVEP-Based BCIs by Within-Subject Information Transfer.* Front. Neurosci., 2022. **16**.

[27] X. Chai, Q. Wang, Y. Zhao, et al., *A Fast, Efficient Domain Adaptation Technique for Cross-Domain Electroencephalography(EEG)-Based Emotion Recognition.* Sensors, 2017. **17**(5).

[28] H. He and D. Wu, *Transfer Learning for Brain–Computer Interfaces: A Euclidean Space Data Alignment Approach.* IEEE Trans. Biomed. Eng., 2020. **67**(2): p. 399-410.

[29] E. Maiorana, *Deep learning for EEG-based biometric recognition.* Neurocomputing, 2020. **410**: p. 374-386.

[30] Y. Miao, W. Jiang, N. Su, et al., *MLDA: Multi-Loss Domain Adaptor for Cross-Session and Cross-Emotion EEG-Based Individual Identification*. IEEE J. Biomed. Health, 2023. **27**(12), p. 5767-5778.

[31] H. Zhao, Y. Wang, Z. Liu, et al., *Individual Identification Based on Code-Modulated Visual-Evoked Potentials.* IEEE Trans. Inf. Forensics Secur., 2019. **14**(12): p. 3206-3216.

[32] F. Di Russo and D. Spinelli, *Electrophysiological evidence for an early attentional mechanism in visual processing in humans.* Vision Res., 1999. **39**(18): p. 2975-2985.

[33] X. Chen, Y. Wang, S. Gao, et al., *Filter bank canonical correlation analysis for implementing a high-speed SSVEP-based brain–computer interface.* J. Neural Eng., 2015. **12**(4).

[34] H. Tanaka, T. Katura, and H. Sato, *Task-related component analysis for functional neuroimaging and application to near-infrared spectroscopy data.* Neuroimage, 2013. **64**: p. 308-327.

[35] M. Nakanishi, Y. Wang, X. Chen, et al., *Enhancing Detection of SSVEPs for a High-Speed Brain Speller Using Task-Related Component Analysis.* IEEE Trans. Biomed. Eng., 2018. **65**(1): p. 104-112.

[36] Q. Wei, S. Zhu, Y. Wang, et al., *A Training Data-Driven Canonical Correlation Analysis Algorithm for Designing Spatial Filters to Enhance Performance of SSVEP-Based BCIs.* Int. J. Neural Syst., 2020. **30**(05).

[37] P.H. Sch¨onemann, *A generalized solution of the orthogonal procrustes problem.* Psychometrika, 1966. **31**(1): p. 1-10.

[38] L. Zheng, W. Pei, X. Gao, et al., *A high-performance brain switch based on code-modulated visual evoked potentials.* J. Neural Eng., 2022. **19**(1).

[39] G. Chandrashekar and F. Sahin, *A survey on feature selection methods.* Computers & Electrical Engineering, 2014. **40**(1): p. 16-28.

[40] V. Bolón-Canedo, N. Sánchez-Maroño, and A. Alonso-Betanzos, *A review of feature selection methods on synthetic data.* Knowledge and Information Systems, 2012. **34**(3): p. 483-519.

[41] Y.J. Wang, M. Nakanishi, Y.T. Wang, et al., *Enhancing Detection of Steady-State Visual Evoked Potentials Using Individual Training Data.* 2014 36th Annual International Conference of the Ieee Engineering in Medicine and Biology Society (Embc), 2014: p. 3037-3040.

[42] L. Van der Maaten and G. Hinton, *Visualizing data using t-SNE.* Journal of machine learning research, 2008. **9**(11).

[43] M. Nakanishi, Y. Wang, Y.-T. Wang, et al., *A High-Speed Brain Speller Using Steady-State Visual Evoked Potentials.* Int. J. Neural Syst., 2014. **24**(06).

[44] X. Chen, Y. Wang, M. Nakanishi, et al., *High-speed spelling with a noninvasive brain–computer interface.* Proceedings of the National Academy of Sciences, 2015. **112**(44).

[45] Y.-T. Wang, M. Nakanishi, Y. Wang, et al., *An online brain-computer interface based on SSVEPs measured from non-hair-bearing areas.* IEEE Trans. Neural Syst. Rehabil. Eng., 2016. **25**(1): p. 14-21.

[46] P. Arnau-Gonzalez, S. Katsigiannis, M. Arevalillo-Herraez, et al., *BED: A New Data Set for EEG-Based Biometrics.* IEEE Internet Things J., 2021. **8**(15): p. 12219-12230.

Hongze Zhao received his B.S. degree in Optical Information Science and Technology from Minzu University of China in 2016, and his M.S. degree in Circuit and System from Institute of Semiconductors, University of Chinese Academy of Sciences in 2019. Following his tenure as a Research Assistant in Y. Wang's lab at Institute of Semiconductors, Chinese Academy of Sciences, he is currently pursuing his Ph.D. degree in Biomedical Engineering at Tsinghua University, Beijing, China. His research interests include EEG Biometrics, Transfer Learning, and Brain-Computer Interface.

Yijun Wang (M'11) received the B.E. and Ph.D. degrees in biomedical engineering from Tsinghua University, Beijing, China, in 2001 and 2007, respectively. From 2008 to 2015, he was a Post-Doctoral Fellow and an Assistant Project Scientist with the Swartz Center for Computational Neuroscience, University of California at San Diego, San Diego, CA, USA. He is currently a Research Fellow with the Institute of Semiconductors, Chinese Academy of Sciences, Beijing. His research interests include brain-computer interface, biomedical signal processing, and machine learning.

Xiaorong Gao received his B.S. degree from Zhejiang University in 1986, M.S. degree from Peking Union Medical College in 1989, and Ph.D. degree from Tsinghua University in 1992, after which he taught at Tsinghua University, where he served as Lecturer, Associate Professor, Professor, and Distinguished Professor. His research interests include brain-computer interface and biomedical signal processing.